

## Electronic Supplementary Information

### **Boronic acid-functionalized molybdenum disulfide quantum dots for the ultrasensitive analysis of dopamine based on synergistic quenching effects from IFE and aggregation**

Xinrong Guo, Jianzhi Huang, Qiang Zeng, Yubo Wei, Xuye Liu, Lishi Wang\*

---

\* Corresponding author. Address: School of Chemistry and Chemical Engineering, South China University of Technology, Guangzhou 510641, China. Phone: +86 020 87112906.

E-mail address: [wanglsh@scut.edu.cn](mailto:wanglsh@scut.edu.cn).

---

**Contents:**

- 1. Experimental part**
- 2. Characterization of B-MoS<sub>2</sub> QDs**
- 3. The direct electronic bandgap of B-MoS<sub>2</sub> QDs and MoS<sub>2</sub> QDs**
- 4. Optical characteristics of MoS<sub>2</sub> QDs**
- 5. pH effect of B-MoS<sub>2</sub> QDs**
- 6. The QY of B-MoS<sub>2</sub> QDs and MoS<sub>2</sub> QDs**
- 7. The fluorescent stable of B-MoS<sub>2</sub> QDs**
- 8. Optimization of the experimental conditions**
- 9. The interfere of metal ions with the dopamine detection process by using B-MoS<sub>2</sub> QDs**
- 10. Fluorescence quenching mechanism of B-MoS<sub>2</sub> QDs toward dopamine**
- 11. The aggregation effect of TEM image for B-MoS<sub>2</sub> QDs with dopamine**
- 12. Detection of various saccharides by using B-MoS<sub>2</sub> QDs**
- 13. The RLS spectra of B-MoS<sub>2</sub> QDs toward various saccharides**
- 14. The FL spectra of B-MoS<sub>2</sub> QDs without and with human serum**
- 15. Summary table of QY for B-MoS<sub>2</sub> QDs**
- 16. Summary table of QY for MoS<sub>2</sub> QDs**
- 17. Summary table of performance comparisons of B-MoS<sub>2</sub> QDs-based system**
- 18. Summary table of IFE calculation of B-MoS<sub>2</sub> QDs toward dopamine**
- 19. Summary table of chemical structures of various saccharides involved in the quenched mechanism**
- 20. Summary table of B-MoS<sub>2</sub> QDs toward dopamine in natural sample**

---

## **1. Experimental part**

### **1.1. Chemicals and materials.**

Sodium molybdate dihydrate ( $\text{Na}_2\text{MoO}_4 \cdot 2\text{H}_2\text{O}$ ), 3-aminobenzenboronic acid (APBA), 1-ethyl-3-(3-dimethylaminopropyl) carbodiimide (EDC) and dopamine hydrochloride (DA) were purchased from J&K Chemical (Beijing, China). All other chemicals (analytical grade) were used without further purification. The doubly distilled water was used throughout the experiments (resistivity: 18.2 M $\Omega$  cm). The normal human serum samples were received from Huayueyang Biotechnology Co. Ltd (Beijing, China).

### **1.2. Apparatus.**

Transmission electron microscopy (TEM) images were recorded on JEOL-2010F microscope (Japan). Atomic force microscopy (AFM) images were obtained on Multimode Nano-scope V scanning probe microscopy (Bruker, Germany). X-ray diffraction (XRD) patterns were taken with a D4 X-ray diffractometer (Bruker, Germany). Fourier transform infrared spectrum (FT-IR) was recorded on Bruker VERTEX 70 spectrometer (Germany). X-ray photoelectron spectroscopy (XPS) measurements were recorded on an ESCALAB 250Xi (Thermo Scientific, America). Dynamic light scattering (DLS) measurements were taken with a Nano Particle Analyzer SZ-100 (HORIBA, Co., USA). Ultraviolet-Visible (UV-vis) spectra were obtained from Hitachi UV-3900H spectrophotometer (Japan). The fluorescence spectra were taken with HORIBA Fluoromax-4 spectrofluorometer (USA). The time-resolved fluorescence decay spectra were recorded on FLS-920 fluorescence spectrophotometer (Edinburgh, English).

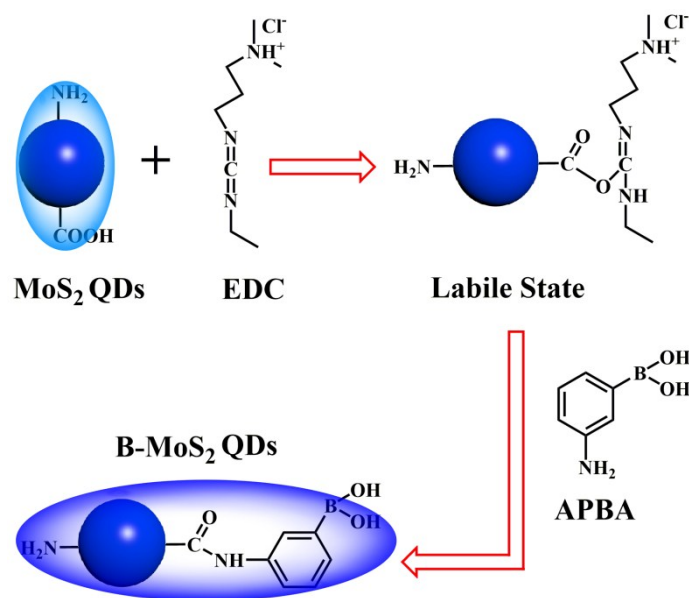
### **1.3. Preparation process of MoS<sub>2</sub> QDs.**

The MoS<sub>2</sub> QDs were synthesized via a simple hydrothermal method by means of Na<sub>2</sub>MoO<sub>4</sub> and *L*-cysteine on the basis of previous report with slight modification.<sup>1</sup> In short, 0.25 g

$\text{Na}_2\text{MoO}_4$  was dissolved in 25 mL doubly distilled water through ultrasound for 5 min, and its pH value was adjusted to near 6.5 through adding 0.1 M HCl. Subsequently, *L*-cysteine (0.5 g) was dissolved into 50 mL doubly distilled water, and then added into the above solution with stirring at room temperature. Thereafter, the mixture was transferred into a Teflon-lined stainless steel autoclave (100 mL capacity), heated and reacted for 36 h at 200 °C. Finally cooling to the ambient temperature, the supernatant was collected via centrifugation at 12000 rpm for 20 min to obtain the pristine  $\text{MoS}_2$  QDs.

#### 1.4. Synthesized Process of B- $\text{MoS}_2$ QDs.

The B- $\text{MoS}_2$  QDs were prepared through a simple amide reaction with some nuances between APBA and as-prepared  $\text{MoS}_2$  QDs.<sup>2</sup> Briefly, the 30 mL of  $\text{MoS}_2$  QDs solution was added in 30 mL phosphate buffered solution (0.2 mol  $\text{L}^{-1}$ , pH 7.4). Then, 180 mg APBA and 240 mg EDC were added into the above mixture, shaking for 3 h in the dark at ambient temperature. After filtering with 0.22  $\mu\text{m}$  microporous membrane, the filtrate was collected to obtain the B- $\text{MoS}_2$  QDs and stored in the refrigerator at 4 °C before use.



**Scheme S1.** Synthetic mechanism of the B- $\text{MoS}_2$  QDs by using as-prepared  $\text{MoS}_2$  QDs and APBA.

---

### **1.5. Determination of DA based on the B-MoS<sub>2</sub> QDs.**

For DA detection process, the B-MoS<sub>2</sub> QDs (25 μL), 950 μL of B-R buffer solution (0.1 mol L<sup>-1</sup>, pH = 8.0) and different concentrations of DA ( $C_{DA}$ : 0-75 μmol L<sup>-1</sup>, total 19) were sequentially added into a 4 mL quartz cell. The mixture was further diluted to final volume of 2.0 mL by means of water. After the solution mixed thoroughly, the relevant FL spectral data was recorded immediately at the ambient temperature under the emission wavelength.

---

## 2. Characterization of B-MoS<sub>2</sub> QDs

The XRD patterns of MoS<sub>2</sub> QDs and B-MoS<sub>2</sub> QDs are shown in Fig. S1B, there has two diffraction peaks locates at 32.4° and 58.3° are respectively assigned to the (100) and (110) phase for MoS<sub>2</sub> QDs and B-MoS<sub>2</sub> QDs.<sup>3</sup> Besides, the characteristic diffraction peak around at 14° ascribes to the (002) phase of MoS<sub>2</sub> is disappeared in both MoS<sub>2</sub> QDs and B-MoS<sub>2</sub> QDs because the layered amounts are very few, resulting in the interlayer action weaken significantly.<sup>4</sup>

Furthermore, the FT-IR spectra of APBA, MoS<sub>2</sub> QDs and B-MoS<sub>2</sub> QDs are exhibited in Fig. S1C. The peaks about at 1630 and 1530 cm<sup>-1</sup> are severally caused by the N-H bending vibration and in-plane N-H stretching vibration in the FT-IR spectrum of MoS<sub>2</sub> QDs.<sup>1</sup> The peak locates at over wide range of 3600–2900 cm<sup>-1</sup> are matched to the N-H/O-H stretching vibration for APBA, MoS<sub>2</sub> QDs and B-MoS<sub>2</sub> QDs, where N-H originated from the reducing agent of *L*-cysteine, denoting that the amino groups and hydroxyl groups are likely to exist on the surface of above three substances.<sup>5</sup> The weak absorption band around at 465 cm<sup>-1</sup> is assigned to the Mo-S vibration for MoS<sub>2</sub> QDs and B-MoS<sub>2</sub> QDs.<sup>6</sup> The major four peaks of APBA and B-MoS<sub>2</sub> QDs locate at 1340, 1187, 1090 and 1020 cm<sup>-1</sup>, are respectively ascribed to B-O stretching vibration, B-O-H bending vibration, C-B stretching vibration and B-O-H deformation vibration, which is consistent with the results of XPS analysis of B 1s spectrum in Fig. 1F.<sup>7,8</sup> Moreover, the amido bond is formed as boronic acid modifies to the MoS<sub>2</sub> QDs surface, resulting in the peak intensity of stretching vibration locates at 1650 cm<sup>-1</sup> is marked improvement.<sup>9</sup> Above result suggests that boric acid functional groups are successfully modified to the MoS<sub>2</sub> QDs surface during amide reaction.

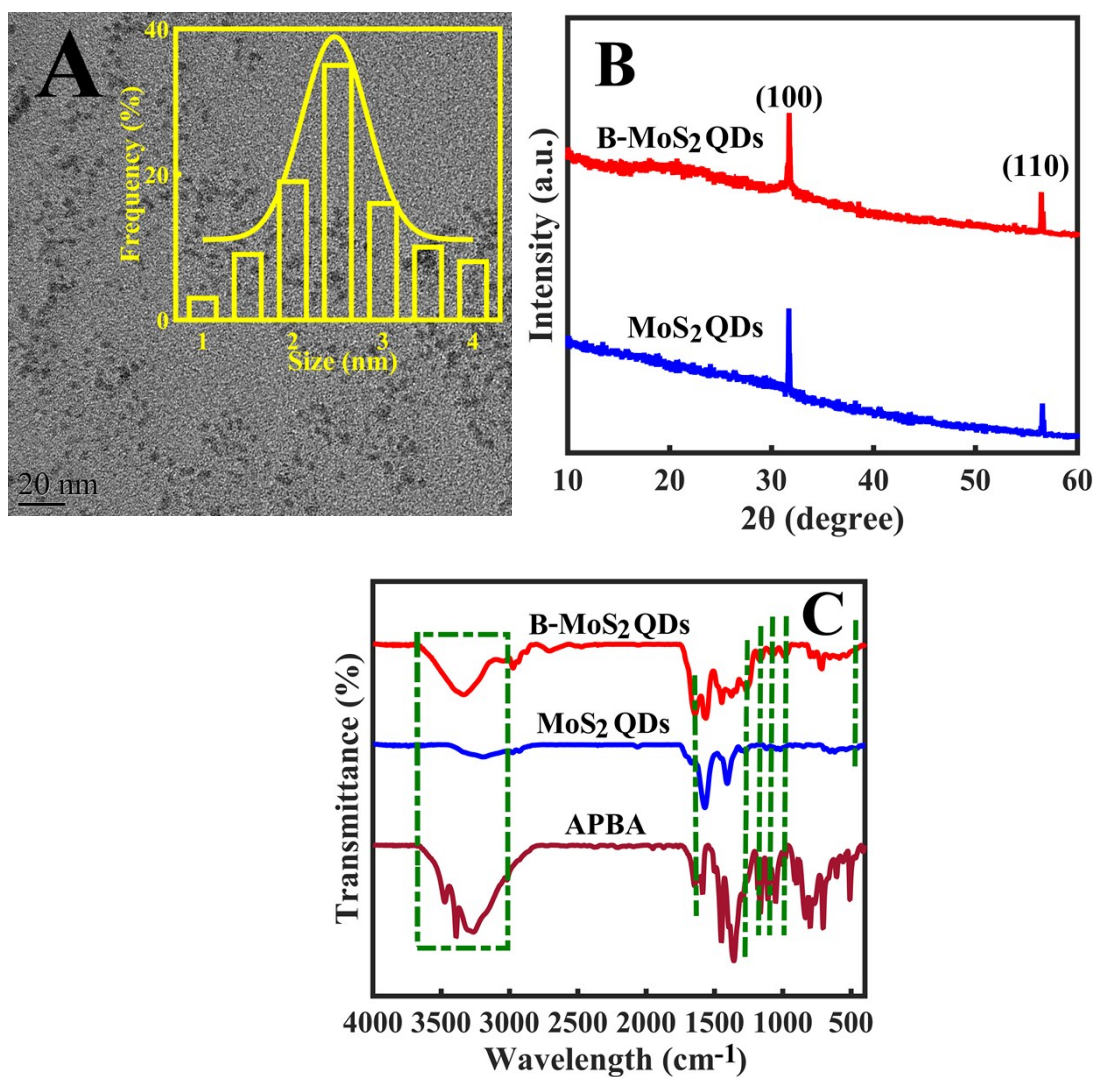


**Fig. S1** (A) TEM image of MoS<sub>2</sub> QDs with diameter distribution. (B) XRD patterns of MoS<sub>2</sub> QDs and B-MoS<sub>2</sub> QDs. (C) FT-IR spectra of APBA, MoS<sub>2</sub> QDs and B-MoS<sub>2</sub> QDs.

### 3. The direct electronic bandgap of B-MoS<sub>2</sub> QDs and MoS<sub>2</sub> QDs

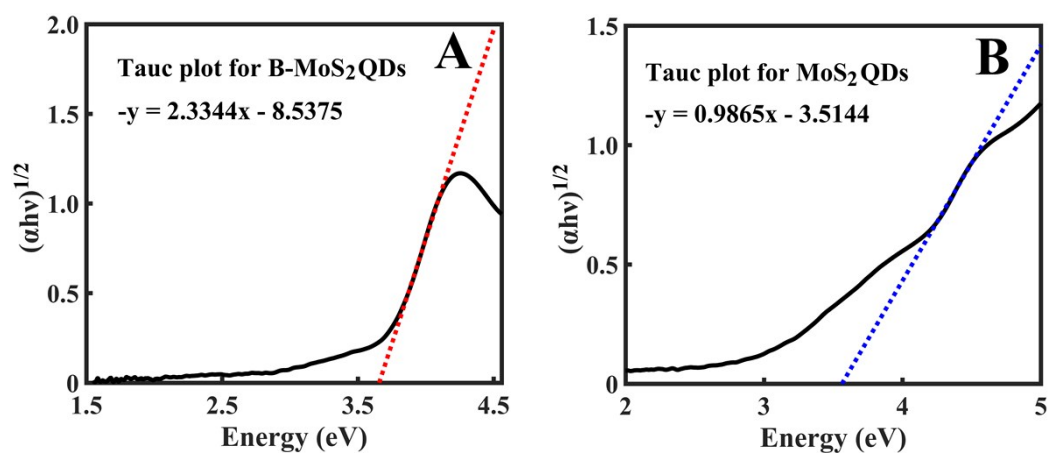


**Fig. S2 (A)** A plot of  $(\alpha h\nu)$  versus photon energy for the B-MoS<sub>2</sub> QDs solution, and the red dashed line is the linear fitting; **(B)** A plot of  $(\alpha h\nu)$  versus photon energy for the MoS<sub>2</sub> QDs solution, and the blue dashed line is the linear fitting.

#### 4. Optical characteristics of MoS<sub>2</sub> QDs

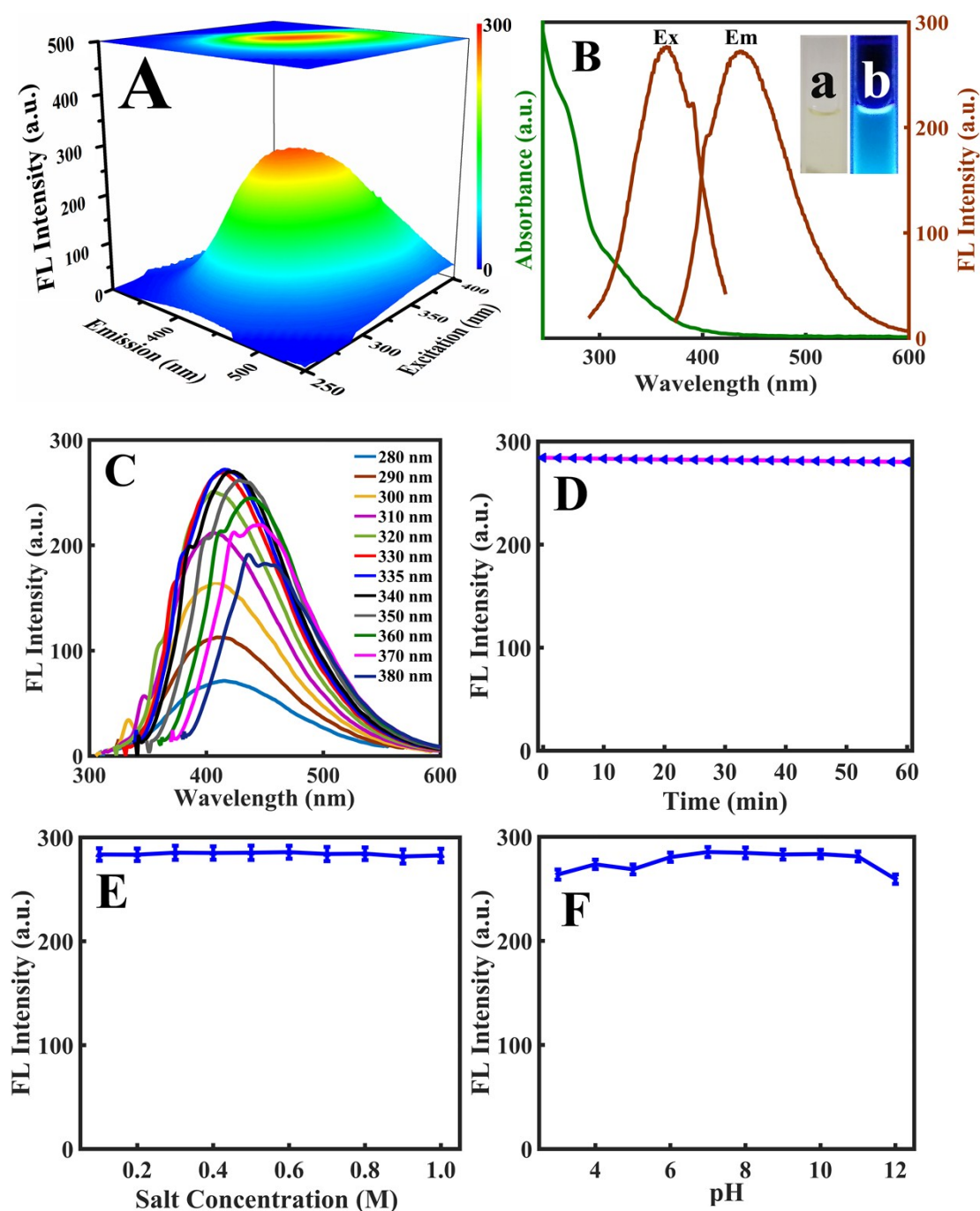


**Fig. S3** (A) 3D FL image of MoS<sub>2</sub> QDs. (B) UV-vis absorption and FL excitation and emission spectra of MoS<sub>2</sub> QDs; **Inset:** photos of MoS<sub>2</sub> QDs under visible and UV light at 365 nm. (C) FL spectra of MoS<sub>2</sub> QDs at over excitation wavelength range of 280 to 380 nm. (D) Photobleaching of MoS<sub>2</sub> QDs under irradiation for one hour. (E) Different salt concentrations effects for MoS<sub>2</sub> QDs. (F) The pH effect for MoS<sub>2</sub> QDs.

## 5. pH effect of B-MoS<sub>2</sub> QDs

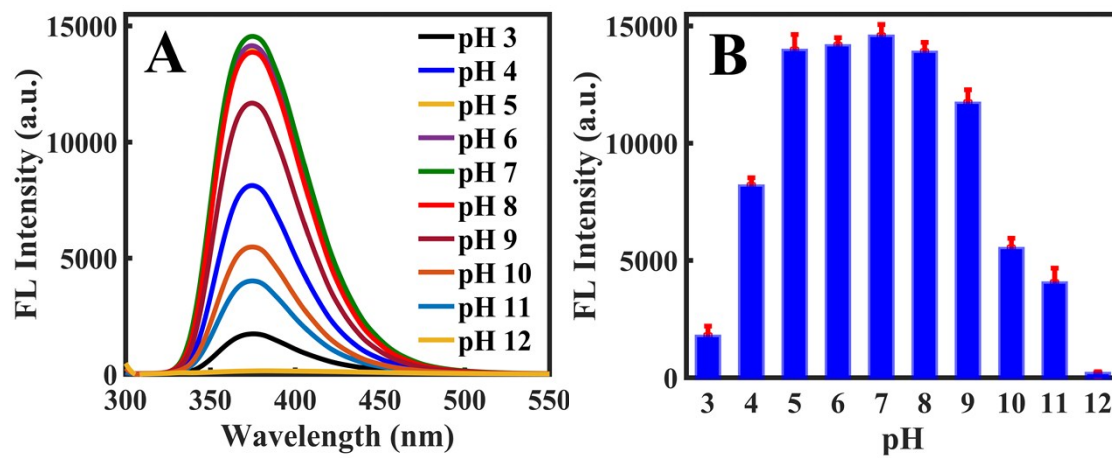


**Fig. S4 (A)** The FL spectra of B-MoS<sub>2</sub> QDs at different pH conditions. **(B)** The pH effect on the FL intensity of B-MoS<sub>2</sub> QDs solution.

## 6. The QY of B-MoS<sub>2</sub> QDs and MoS<sub>2</sub> QDs

Additionally, the quantum yields (QY) of B-MoS<sub>2</sub> QDs and MoS<sub>2</sub> QDs samples were calculated with the use of the integrated FL intensity (Figure S4). The quinine sulfate is selected as the reference standard, and the equation used for calculations is<sup>10</sup>:

$$QY_{test} = QY_{QS} \times \frac{S_{test}}{S_{QS}} \times \frac{\eta_{test}^2}{\eta_{QS}^2}$$

Where the subscripts “QS” and “test” respectively stand for quinine sulphate and test materials contain MoS<sub>2</sub> QDs and B-MoS<sub>2</sub> QDs; S is the slope of the fluorescence intensity versus the absorbance plot, and  $\eta$  is the refractive index of the solvent. From the Table S1 and S2, the QY of the B-MoS<sub>2</sub> QDs is calculated to be 31.6%, which is 21.1 times that of MoS<sub>2</sub> QDs (1.5%). This denotes that the FL improvement of B-MoS<sub>2</sub> QDs is owed to the functional effect of APBA.

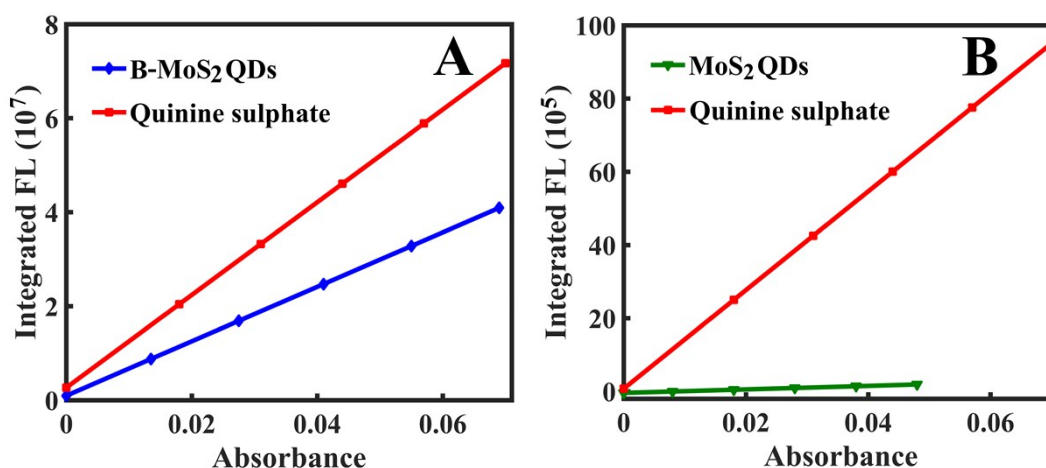


**Fig. S5 (A)** Linear plots of integrated FL intensity versus absorbance for two samples of quinine sulphate and B-MoS<sub>2</sub> QDs, respectively. **(B)** Linear plots of integrated FL intensity versus absorbance for two samples of quinine sulphate and MoS<sub>2</sub> QDs, respectively.

## 7. The fluorescent stable of B-MoS<sub>2</sub> QDs

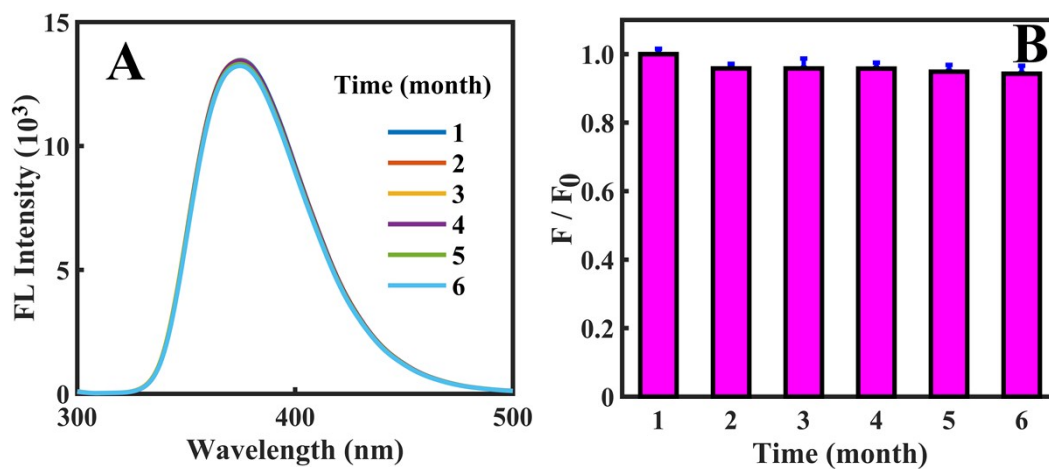


**Fig. S6** (A) The FL spectra of B-MoS<sub>2</sub> QDs at different storage time (six months). (B) The storage time effect on the FL intensity of B-MoS<sub>2</sub> QDs.

---

## 8. Optimization of the experimental conditions

The experimental conditions, contained reaction time and pH of medium, were proposed for illustrated and optimized in Fig. S7, the sample was composed of B-MoS<sub>2</sub> QDs and 35  $\mu\text{mol L}^{-1}$  DA were added in B-R buffer (pH 8.0), and collected FL intensity spectral data of each minute at 375 nm. It is observed that after adding DA solution, the FL intensity is immediately quenched within 1 min; thereafter, the FL intensity tends to be stable over the time range from 1.0 to 10 min, demonstrating that the quenching effect of DA toward B-MoS<sub>2</sub> QDs is quick (Fig. S7A, B). This also implies that a rapid and sensitive detection method for DA is constructed.

Moreover, we also investigated the pH effect for the B-MoS<sub>2</sub> QDs toward DA. The different pH of B-R buffers over the range from 5.0 to 10.0 is regarded as the medium to detect DA. As shown in Fig. S7C, with increasing pH of medium, the FL intensity of B-MoS<sub>2</sub> QDs gradually reduces in the presence of DA. Additionally, the FL intensity difference value (D-value), compared with FL intensity of B-MoS<sub>2</sub> QDs in absence and the presence of DA, increases gradually from pH 5.0 to 8.0, and reaches the maximum as the pH 8.0; thereafter, which is gradually decreased over the pH range from 8.0 to 10.0 (Fig. S7D). The results indicate that the optimal experimental pH is set to 8.0.

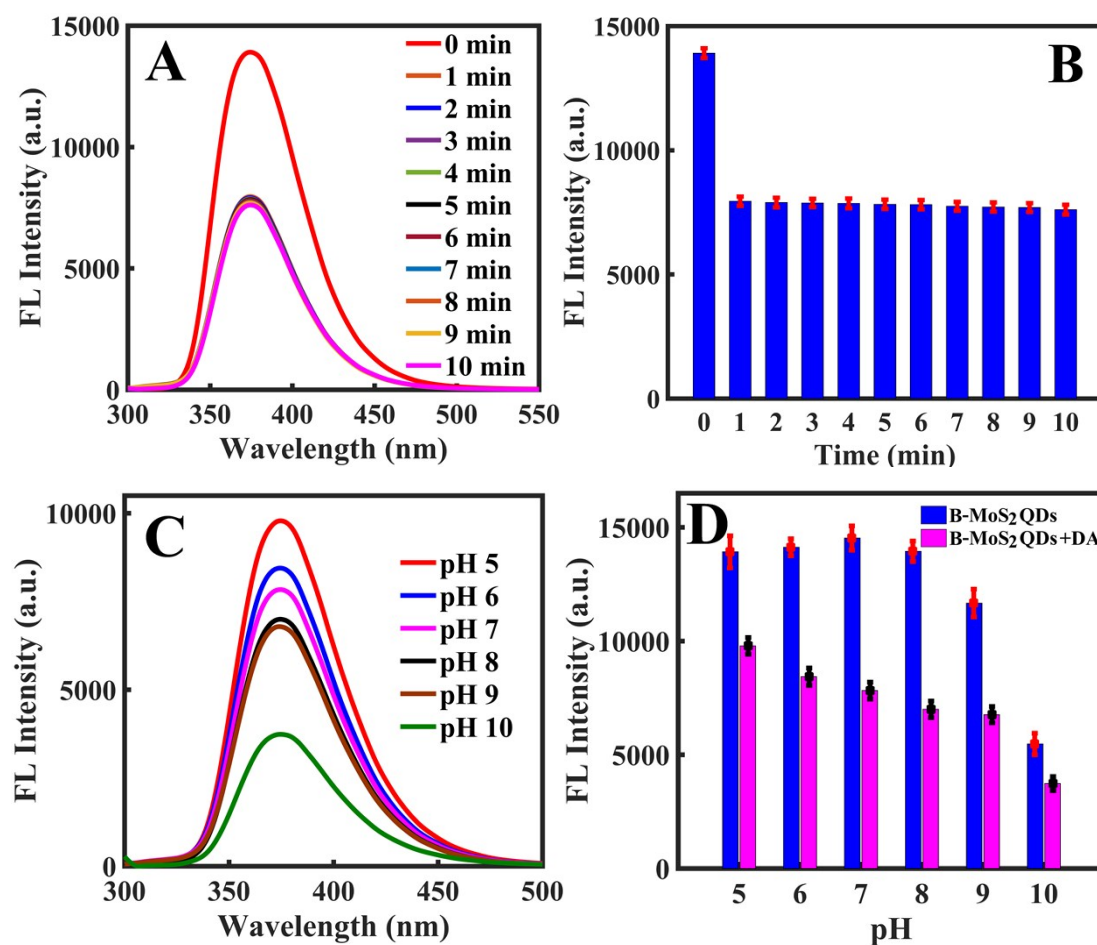


**Fig. S7** (A) FL spectra of B-MoS<sub>2</sub> QDs toward DA with different reaction times. (B) Time effect on the FL intensity of B-MoS<sub>2</sub> QDs with DA (35  $\mu\text{mol L}^{-1}$ ). (C) FL spectra of B-MoS<sub>2</sub> QDs with DA at different pH conditions. (D) The pH effect on the FL spectra of B-MoS<sub>2</sub> QDs in the absence and presence of DA (35  $\mu\text{mol L}^{-1}$ ).

---

9. The interfere of metal ions with the dopamine detection process by using B-MoS<sub>2</sub> QDs

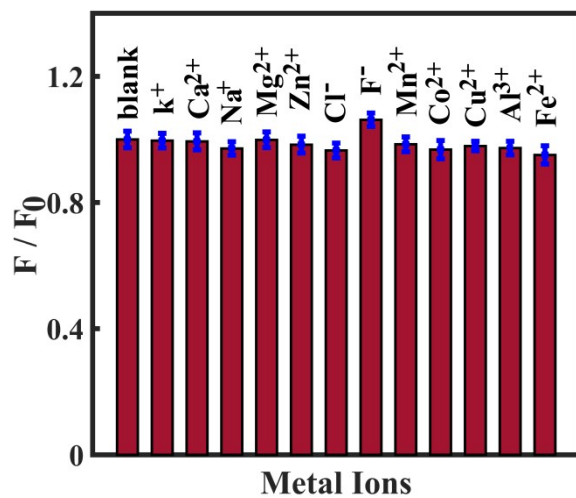


**Fig. S8** Selectivity study of B-MoS<sub>2</sub> QDs toward DA in the presence of various metal ions, of which concentration is 60  $\mu\text{mol L}^{-1}$ .

## 10. Fluorescence quenching mechanism of B-MoS<sub>2</sub> QDs toward dopamine

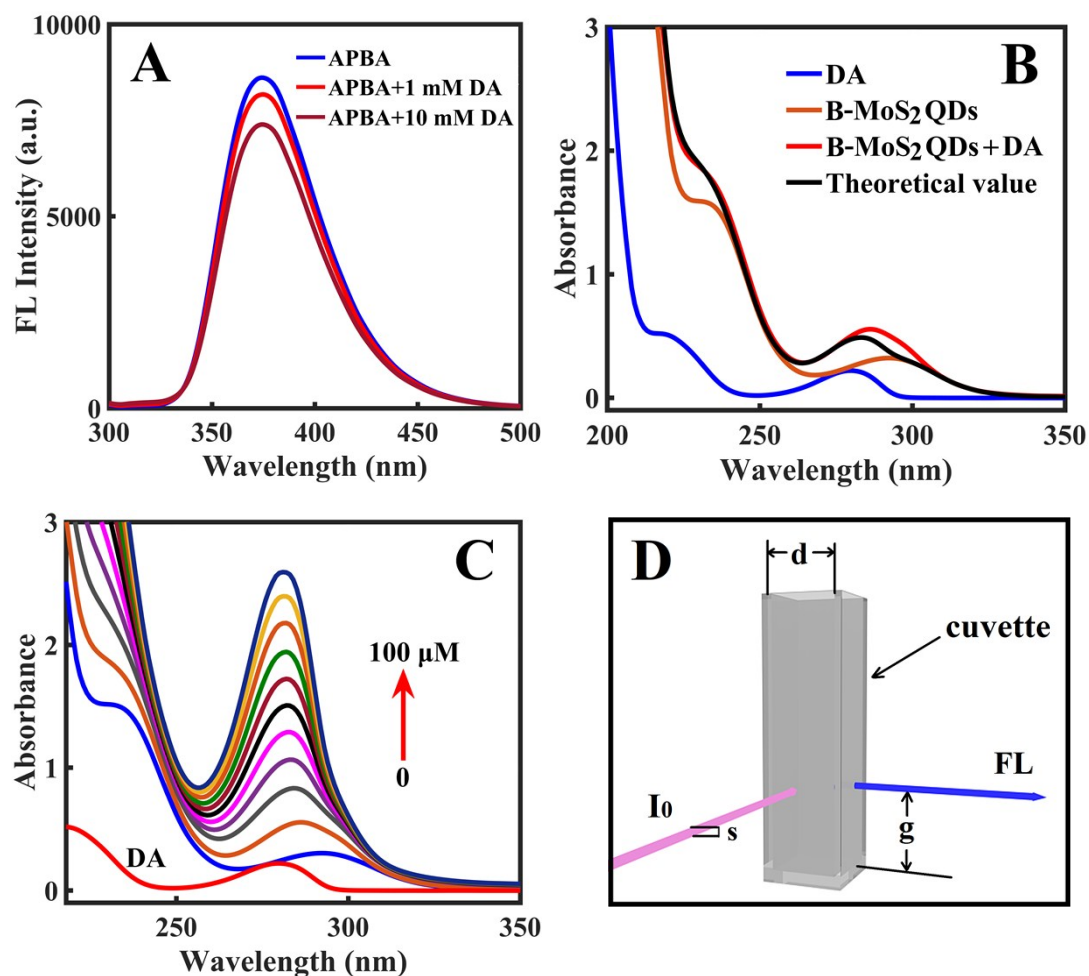


**Fig. S9.** (A) FL spectra of APBA, APBA and DA with different concentrations. (B) UV-vis absorption spectra of DA, B-MoS<sub>2</sub> QDs, the theoretical and experimental spectra of the sum of B-MoS<sub>2</sub> QDs and DA. (C) UV-vis absorption spectra of B-MoS<sub>2</sub> QDs with DA over concentration range of 0-100  $\mu\text{mol L}^{-1}$ . (D) Schematic diagram of cuvette geometry for IFE. The pink line represents the excitation beam and its thickness is 0.1 cm ( $s$ ); the blue line represents the observed FL from the fluorescence beam;  $d$  is the inner diameter of the cuvette (1.0 cm);  $g$  is the distance between the edge of the excitation beam and the edge of the cuvette (0.4 cm).

---

**11. The aggregation effect of TEM image for B-MoS<sub>2</sub> QDs toward dopamine**

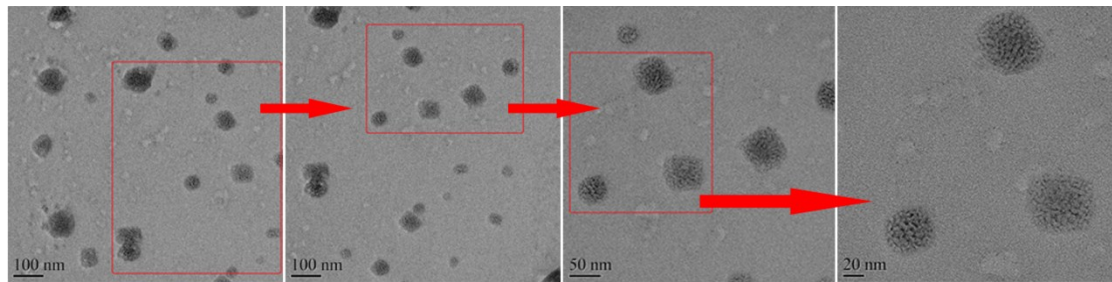


**Fig. S10** The different magnifications of TEM image about B-MoS<sub>2</sub> QDs with dopamine.

---

## 12. Detection of various saccharides by using B-MoS<sub>2</sub> QDs.

Boronic acid can react with cis-diols to form stable boronate complexes.<sup>11,12</sup> Thus, the saccharides such as glucose, fructose, sucrose and lactose are also detected by using of the B-MoS<sub>2</sub> QDs. The FL intensity of B-MoS<sub>2</sub> QDs is not efficient and rapid quenching by four saccharides under B-R buffer solution (pH = 8.0). This may be ascribed to the reaction between boronic acid and sugar is a slow reaction process. Therefore, on the basis of previous report, we choose the reaction time is 120 min.<sup>11</sup> In Fig. S11A, B, C and D, the FL intensity of B-MoS<sub>2</sub> QDs reaches to maximum value as the emission wavelength at 375 nm ( $F_0$ ), however, it will gradually decrease after respectively adding glucose, fructose, sucrose and lactose with all of the concentrations range from 0 to 100  $\mu\text{mol L}^{-1}$  (F), and records the calibration curve between quenched ratio  $(F_0 - F) / F$  and concentrations of aforementioned four sugars (inset in Fig. S11A, B, C and D). Simultaneously, compared with the calibration curve of each sugar, the recognition effect of glucose is better than other three saccharides by using the B-MoS<sub>2</sub> QDs, and the order of quenching effect is glucose  $\gg$  fructose  $>$  sucrose  $>$  lactose (Fig. S11E). This may be caused by the different chemical structure of saccharides (Table S5). Compared with the chemical structure of other three sugars, glucose contains two pairs cis conformational diol unit, which can cross-link the B-MoS<sub>2</sub> QDs, resulting in fluorescence quenching well.<sup>13</sup> In addition, the quenching mechanisms of B-MoS<sub>2</sub> QDs toward four saccharides were investigated by means of RLS. From the Fig. S12, it is clearly observed that the intensity of RLS peak ranged from 300 to 600 nm is increased when severally adding four sugars with the concentration is 100  $\mu\text{mol L}^{-1}$ , manifesting that the B-MoS<sub>2</sub> QDs can assemble together with assistance of the saccharides through the crosslinked action between boronic acid and cis-diols. Moreover, the order of increased intensity of RLS peak is glucose  $>$  fructose  $>$  sucrose  $>$  lactose, which is consistent with the order of fluorescent quenching effect. These results indicate that glucose can better quench fluorescence of B-MoS<sub>2</sub> QDs, due to the surface quenching states induced mechanism that is the coupled effect between boronic acids and cis-diols.

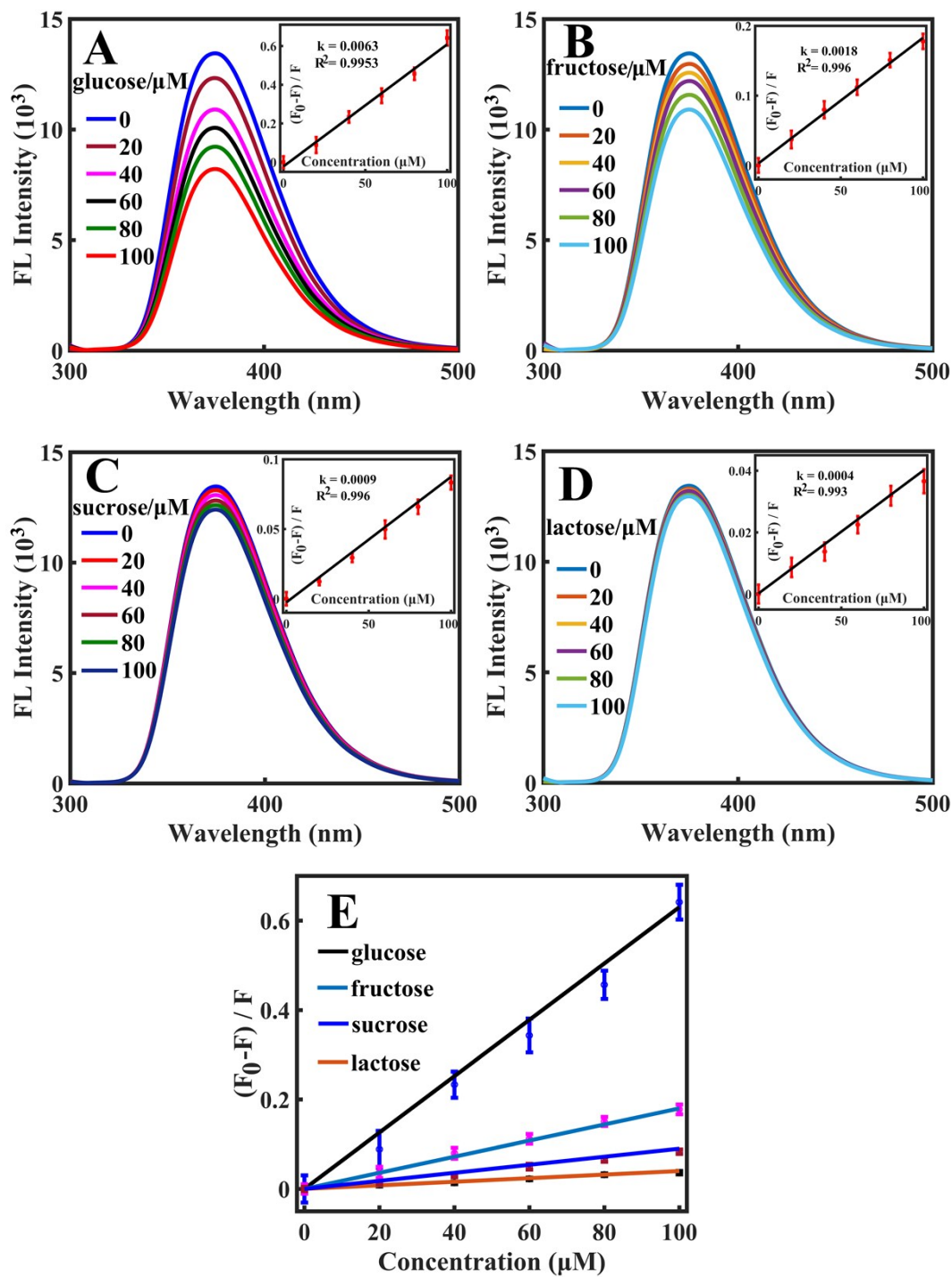


**Fig. S11** FL spectra of B-MoS<sub>2</sub> QDs toward (A) glucose, (B) fructose, (C) sucrose and (D) lactose with diverse concentrations (0–100  $\mu\text{mol L}^{-1}$ ). Inset: Calibration curve of  $(F_0 - F) / F$  versus four saccharides concentration. (E) Compared with the calibration curve of  $(F_0 - F) / F$  versus four saccharides concentration (0–100  $\mu\text{mol L}^{-1}$ ).

13. The RLS spectra of B-MoS<sub>2</sub> QDs toward various saccharides

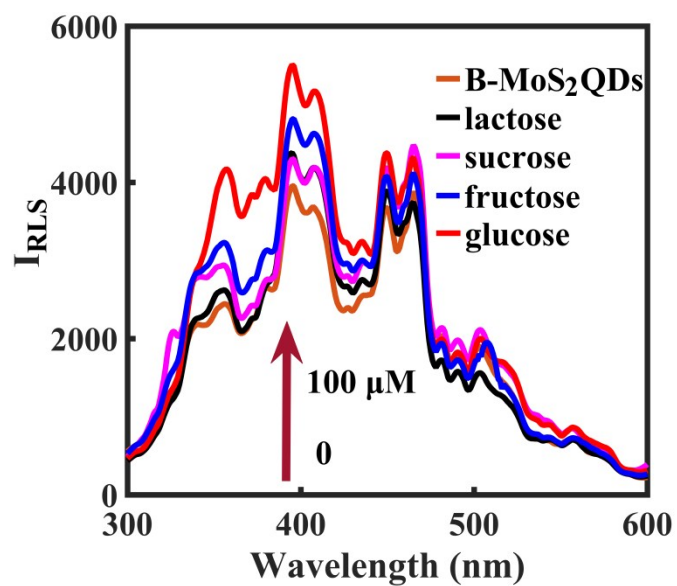


**Fig. S12.** RLS spectra of B-MoS<sub>2</sub> QDs in the absence and existence of four saccharides (all of their concentrations were 100 μmol L<sup>-1</sup>).

14. The FL spectra of B-MoS<sub>2</sub> QDs without and with human serum

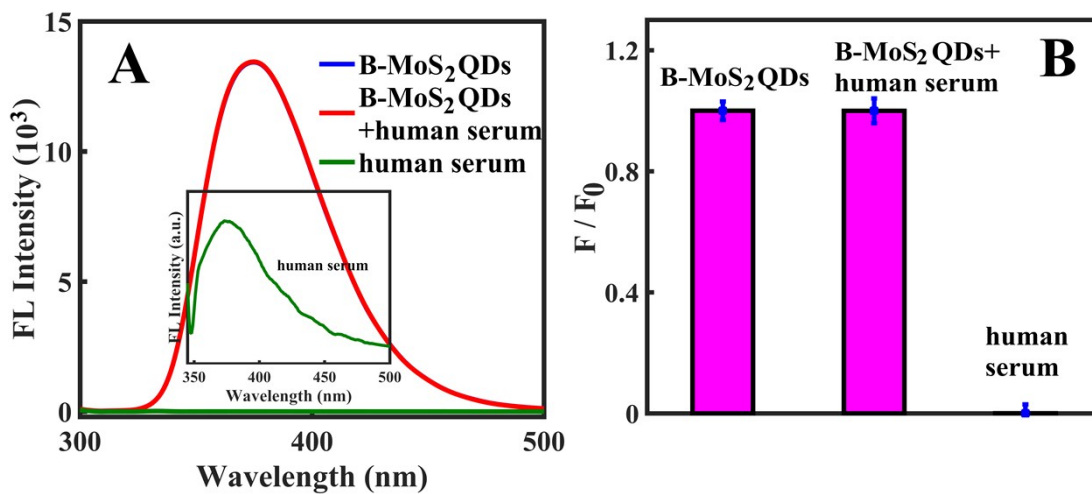


**Fig. S13.** (A) FL spectra of B-MoS<sub>2</sub> QDs in the absence and existence of human serum; inset: FL spectrum of human serum under the excitation wavelength of 300 nm. (B) The FL intensity effect of B-MoS<sub>2</sub> QDs in the presence of human serum.

---

## 15. Summary table of QY for B-MoS<sub>2</sub> QDs

**Table S1** Quantum yield of B-MoS<sub>2</sub> QDs

---

Sample	Slope of integrated FL	Recovery (%)	Quantum yield (QY)
Quinine sulphate	13.91×10 <sup>6</sup>	99.07	54.0 %
B-MoS <sub>2</sub> QDs	8.13×10 <sup>6</sup>	99.89	31.6 %

---

---

## 16. Summary table of QY for MoS<sub>2</sub> QDs

**Table S2** Quantum yield of MoS<sub>2</sub> QDs.

Sample	Slope of integrated FL	Recovery (%)	Quantum yield (QY)
Quinine sulphate	17.52×10 <sup>5</sup>	99.77	54.6 %
MoS <sub>2</sub> QDs	4.8×10 <sup>4</sup>	99.83	1.50 %

## 17. Summary table of performance comparisons of B-MoS<sub>2</sub> QDs-based system.

**Table S3** Performance differences of as-prepared fluorescent sensor with other detection methods for analysis of DA.

Method	Probe	Reaction Time (min)	Linear Range (μM)	LOD (μM)	Quench Mechanism	Ref.
Colorimetry	βCD-AuNPs <sup>a</sup>	30	0.02–0.25	0.003	Growth Au assemblies	<b>14</b>
Colorimetry	H-TSIL-AgNPs <sup>b</sup>	10	0.1–7.5	0.031	morphological transition and etching strategy	<b>15</b>
ECL	Cu@CdInSNCs <sup>c</sup>	– <sup>f</sup>	0.5–100	0.355	–	<b>16</b>
ECL	Met-Au NCs <sup>d</sup>	–	0.1–4.0	0.032	–	<b>17</b>
FL/quenched	C2-F127 NPs <sup>e</sup>	90	0.1–10	0.035	PCT <sup>g</sup>	<b>18</b>
FL/dual sign	NaGdF <sub>4</sub> :TbNPs	5	0–20	0.03	ET <sup>h</sup>	<b>19</b>
FL/quenched	MoS <sub>2</sub> QDs	15	0.1–2.5/2.5–100	0.01	IFE <sup>i</sup> and ET	<b>20</b>
FL/quenched	B-MoS <sub>2</sub> QDs	<1	0.25–35	0.087	IFE and AQ <sup>j</sup>	<b>This work</b>

<sup>a</sup>: Natural beta-cyclodextrin modified Au nanoparticles

<sup>b</sup>: Hexagonal platelet shaped silver nanoparticles (Ag NPs) functionalized with task-specific ionic liquid (TSIL)

<sup>c</sup>: Precise mono-Cu<sup>+</sup> ion doped Cd–In–S supertetrahedral chalcogenide nanoclusters

<sup>d</sup>: methionine stabilized gold nanocluster modified glassy carbon electrode

<sup>e</sup>: Novel fluorescent organic nanoparticles (FONs) composed of an arbitrarily selected organic dye (C2) and an amphiphilic triblock copolymer

<sup>f</sup>: Not referred in the references

<sup>g</sup>: Photo-induced charge transfer

<sup>h</sup>: Energy-transfer processes

<sup>i</sup>: Inner filter effect

<sup>j</sup>: Aggregation quenching

---

## 18. Summary table of IFE calculation of B-MoS<sub>2</sub> QDs toward dopamine

**Table S4** IFE of DA on the fluorescence of B-MoS<sub>2</sub> QDs

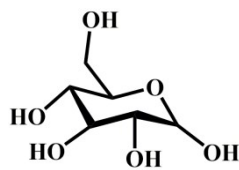
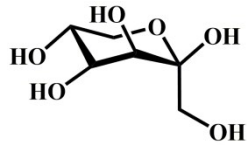
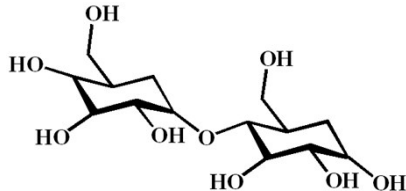
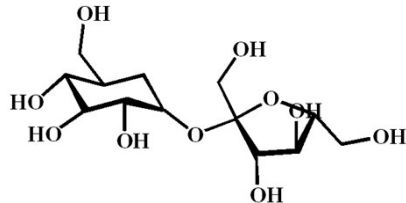
DA/ $\mu$ M	A <sub>ex</sub>	A <sub>em</sub>	CF	F <sub>obs</sub>	F <sub>cor</sub>	F <sub>cor,0</sub> /F <sub>cor</sub>	E <sub>obs</sub>	E <sub>cor</sub>
0	0.2685	0.0038	1.3430	1343.3	1804.1	1	0	0
0.25	0.2798	0.005	1.3604	1327.0	1805.4	0.9993	0.0121	-0.0006
3	0.2835	0.014	1.3785	1299.8	1791.8	1.0069	0.0323	0.0068
6	0.2978	0.029	1.4207	1240.0	1761.7	1.0241	0.0769	0.0235
8	0.2994	0.0304	1.4251	1217.9	1735.7	1.0394	0.0933	0.0379
12	0.328	0.0388	1.4798	1145.3	1694.9	1.0645	0.1474	0.0606
16	0.36	0.0402	1.5302	1081.9	1655.5	1.0898	0.1946	0.0823
20	0.387	0.0418	1.5748	1022.4	1609.4	1.1210	0.2389	0.1079
24	0.4483	0.0421	1.6711	945	1579.2	1.1424	0.2965	0.1247
29	0.5029	0.0433	1.7618	877.2	1545.5	1.1673	0.3470	0.1433
35	0.6134	0.0441	1.9501	774.6	1510.5	1.1944	0.4234	0.1628

---

---

**19. Summary table of chemical structures of various saccharides involved in the quenched mechanism**

**Table S5** chemical structures of various saccharides involved in the quenched mechanism.

Compound	Molecular formula	Molecular weight	Structure
D-glucose	$C_6H_{12}O_6$	180.16	
D-fructose	$C_6H_{12}O_6$	180.16	
lactose	$C_{12}H_{22}O_{11}$	342.30	
sucrose	$C_{12}H_{22}O_{11}$	342.30	

---

---

## 20. Summary table of B-MoS<sub>2</sub> QDs toward dopamine in natural sample

**Table S6** Analysis of DA by using of B-MoS<sub>2</sub> QDs in human serum samples

Sample	Added ( $\mu\text{mol L}^{-1}$ )	Found ( $\mu\text{mol L}^{-1}$ )	Recovery (%)	RSD (% , n=3)
Human serum	10	9.1	91.0	8.1
	20	18.8	94.0	9.4
	30	28.1	93.7	6.2

---

## References

- 1 Y. Wang, Y. N. Ni, *Anal. Chem.*, 2014, **86**, 7463–7470.
- 2 Z. -B. Qu, X. G. Zhou, L. Gu, R. M. Lan, D. D. Sun, D. J. Yu, G. Y. Shi, *Chem. Commun.*, 2013, **49**, 9830–9832.
- 3 W. Gu, Y. H. Yan, C. L. Zhang, C. P. Ding, Y. Z. Xian, *ACS Appl. Mater. Interfaces*, 2016, **8**, 11272–11279.
- 4 H. S. S. Matte, A. Gomathi, A. K. Manna, D. J. Late, R. Datta, S. K. Pati, C. N. R. Rao, *Angew. Chem. Int. Ed.*, 2010, **49**, 4059–4062.
- 5 J. -W. Liu, Y. -M. Wang, L. Xu, L. -Y. Duan, H. Tang, R. -Q. Yu, J. -H. Jiang, *Anal. Chem.*, 2016, **88**, 8355–8358.
- 6 K. J. Huang, L. Wang, Y. J. Liu, Y. M. Liu, H. B. Wang, T. Gan, L. L. Wang, *Int. J. Hydrogen Energy*, 2013, **38**, 14027–14034.
- 7 Y. T. Wang, X. Hai, S. E. M. L. Chen, T. Yang, J. H. Wang, *Nanoscale*, 2018, **10**, 4913–4923.
- 8 Y. H. Liu, W. X. Duan, W. Song, J. J. Liu, C. L. Ren, J. Wu, D. Liu, H. L. Chen, *ACS Appl. Mater. Interfaces*, 2017, **9**, 12663–12672.
- 9 F. W. Li, S. F. Zhao, L. Chen, A. Khan, D. R. MacFarlane, J. Zhang, *Energy Environ. Sci.*, 2016, **9**, 216–223.
- 10 Y. J. Tong, L. D. Yu, L. L. Wu, S. P. Cao, R. P. Liang, L. Zhang, X. H. Xia, J. D. Qiu, *Chem. Commun.*, 2018, **54**, 7487–7490.
- 11 P. F. Shen, Y. S. Xia, *Anal. Chem.*, 2014, **86**, 5323–5329.
- 12 M. B. Lerner, N. Kybert, R. Mendoza, R. Villechenon, M. A. B. Lopez, A. T. C. Johnson, *Appl. Phys. Lett.*, 2013, **102**, 183113–183116.
- 13 Y. Liu, C. M. Deng, L. Tang, A. J. Qin, R. R. Hu, J. Z. Sun, B. Z. Tang, *J. Am. Chem. Soc.*, 2011, **133**, 660–663.
- 14 D. Wen, W. Liu, A. K. Herrmann, D. Haubold, M. Holzschuh, F. Simon, A. Eychmüller, *Small*, 2016, **12**, 2439–2442.
- 15 S. Rostamia, A. Mehdinia, A. Jabbari, E. Kowsari, R. Niroumand, T. J. Booth, *Sensor Actuat. B-Chem.*, 2018, **271**, 64–72.
- 16 F. Wang, J. Lin, H. Y. Wang, S. S. Yu, X. Q. Cui, A. Ali, T. Wu, Y. Liu, *Nanoscale*, 2018, **10**, 15932–15937.
- 17 H. Peng, H. Deng, M. Jian, A. Liu, F. Bai, X. Lin, W. Chen, *Microchim. Acta*, 2017, **184**, 735–743.
- 18 L. Ding, Z. Qin, C. Xiang, G. Zhou, *J. Mater. Chem. B*, 2017, **5**, 2750–2756.
- 19 X. C. Ling, R. K. Shi, J. Zhang, D. M. Liu, M. R. Weng, C. W. Zhang, M. Lu, X. J. Xie, L. Huang, W. Huang, *ACS Sens.*, 2018, **3**, 1683–1689.
- 20 X. N. Liu, W. T. Zhang, L. J. Huang, N. Hu, W. Liu, Y. N. Liu, S. H. Li, C. Y. Yang, Y. R. Suo, J. L. Wang, *Microchim. Acta*, 2018, **185**, 234–241.